

GPA33-pretargeted radioimmunotherapy with mono- and bivalent DOTA-based Lu-177-labeled radiohaptens in a mouse orthotopic liver xenograft model of metastatic human colorectal cancer

Authors:

Alexandre B. Le Roux¹, Edward K. Fung², Sang Gyu Lee¹, Sebastien Monette³, Hong Xu⁴, Hong-Fen Guo⁴, Guangbin Yang⁵, Ouathék Ouerfelli⁵, Achim Jungbluth⁶, Heiko Schöder^{1,2}, Steven M. Larson^{1,2,7}, Nai-Kong V. Cheung⁴, Darren R. Veach^{*1,2}, and Sarah M. Cheal^{*2,7}

Author Affiliations:

¹ Department of Radiology, Memorial Sloan Kettering Cancer Center, New York, NY

² Department of Radiology, Weill Cornell Medicine, New York, NY

³ Laboratory of Comparative Pathology, Memorial Sloan Kettering Cancer Center, Weill Cornell Medicine, and Rockefeller University, New York, NY

⁴ Department of Pediatrics, Memorial Sloan Kettering Cancer Center, New York, NY

⁵ Organic Synthesis Core Facility, Memorial Sloan Kettering Cancer Center, New York, NY

⁶ Department of Pathology, Memorial Sloan Kettering Cancer Center, New York, NY

⁷ Molecular Pharmacology Program, Memorial Sloan Kettering Cancer Center, New York, NY

* Contributed equally to this work

Corresponding author:

Darren R. Veach

Memorial Sloan Kettering Cancer Center

408 East 69th Street

Z-2041

New York, NY 10021

veachd@mskcc.org

ABSTRACT

Rationale: Pretargeted radioimmunotherapy (PRIT), which combines systemic antibody-based targeting with ionizing radiation, is promising for treating liver metastases in patients with colorectal cancer (CRC). Previously, we established a three-step DOTA-PRIT regimen to deliver DOTA radiometal payloads to CRC using an anti-tumor/anti-DOTA bispecific antibody (BsAb) targeting cell surface glycoprotein A33 (GPA33), a tumor antigen target expressed on over 95% of primary and metastatic CRC; a clearing agent; and a monovalent ^{177}Lu radiohapten called [^{177}Lu]Lu-ABD. More recently, we developed a bivalent ^{177}Lu radiohapten called [^{177}Lu]Lu-Gemini to enhance tumor uptake and radiohapten retention. Here, we aimed to compare the efficacy and safety of bivalent vs. monovalent three-step DOTA-PRIT regimens in orthotopic CRC liver metastasis models, to mimic a clinical path forward.

Methods: We established two orthotopic CRC liver metastasis models by inoculating either SW1222-luc (GPA33^{high}) or LoVo (GPA33^{low}) human CRC cells in athymic nude mice under ultrasonographic guidance. Tumor targeting efficacy and dosimetry of the radiohaptens were compared using ex vivo biodistribution studies, SPECT/CT, and quantitative autoradiography. We also performed a DOTA-PRIT experiment to compare the efficacy and safety profiles of bivalent (single-cycle [^{177}Lu]Lu-Gemini, 48 h pretargeting interval) vs. monovalent (multicycle [^{177}Lu]Lu-ABD, 24 h pretargeting interval) three-step DOTA-PRIT regimens, each designed to deliver comparable total radiation doses to tumors (around 50 Gy).

Results: Both radiohaptens demonstrated efficient SW1222-luc tumor targeting, with [^{177}Lu]Lu-Gemini showing superior targeting and tumor activity retention compared with [^{177}Lu]Lu-ABD. In LoVo tumors, [^{177}Lu]Lu-Gemini showed superior targeting, while [^{177}Lu]Lu-ABD showed negligible targeting. Dosimetry estimates revealed higher SW1222-luc tumor mean absorbed doses for [^{177}Lu]Lu-Gemini (119.88 cGy/MBq, 48 h pretargeting interval) compared with [^{177}Lu]Lu-ABD (32.88 cGy/MBq, 24 h pretargeting interval), with more favorable blood and kidney therapeutic indices (50 and 9 for [^{177}Lu]Lu-Gemini, and 15 and 5 for [^{177}Lu]Lu-ABD, respectively). In the DOTA-PRIT experiment, both monovalent (injected activity: 3×44.4 MBq, 133.2 MBq total) and bivalent (injected activity: 44.4 MBq total) radiohapten regimens increased the median survival of treated mice compared with controls: 71 days for [^{177}Lu]Lu-ABD-treated mice, 81 days for [^{177}Lu]Lu-Gemini-treated mice, and 18 days for controls, without a statistical difference between treatment groups. Treatments were well tolerated, without significant weight loss or hematologic changes. Radiation-induced injuries were not identified histologically in the kidneys or bone marrow of mice submitted for necropsy.

Conclusions: Our study demonstrates the exceptional benefit of a multivalent radiohapten strategy when treating an advanced model of CRC liver metastasis. Three-step GPA33 DOTA-PRIT with ^{177}Lu -Gemini demonstrated that multivalency 1) improves PRIT therapeutic indices for blood and kidney and 2) has the potential to greatly reduce the administered activity without compromising the efficiency of the PRIT platform in clinically relevant models of target-rich and target-poor metastatic CRC.

Keywords: multivalent radiohapten; Lu-177; theranostics; colorectal cancer hepatic metastasis; pretargeted radioimmunotherapy

INTRODUCTION

Tumor metastasis is the leading cause of mortality in patients with colorectal cancer (CRC), with the liver being the most common metastatic site, accounting for 70% of all cases [1-4]. About 20–25% of patients with CRC already have metastasis at diagnosis, and an additional 20% will develop metachronous metastasis within three years after diagnosis, limiting surgical cure [5-7]. Indeed, conventional therapies have shown limited efficacy for treating metastatic CRC [5, 7, 8]. Thus, innovative systematic therapies are being developed as alternatives to conventional therapy to improve patient outcomes. In this context, pretargeted radioimmunotherapy (PRIT) is one such targeted treatment approach being developed that has shown promise in the experimental setting.

In PRIT, the slow antibody distribution phase is separated from the radioactive payload, thus enhancing tumor specificity while reducing off-target radiation exposure compared with conventional radioimmunotherapy using a radioimmunoconjugate [9]. PRIT has shown success in targeting the A33 glycoprotein (GPA33), a tumor-associated transmembrane antigen expressed in 95% of primary and metastatic CRC [10-14]. Our current anti-GPA33 β -DOTA-PRIT ("DOTA-PRIT") regimen consists of three steps: the injection of an IgG-scFv anti-GPA33/anti-DOTA bispecific antibody (BsAb), followed 20 h later by the injection of a clearing agent to remove unbound BsAbs from the blood, and finally, 24 h after initial BsAb administration, by the injection of a monovalent radiohaptent, [^{177}Lu]Lu-ABD (also referred as [^{177}Lu]Lu-DOTA-Bn in the literature). [^{177}Lu]Lu-ABD is formed by a complex of lutetium-177 (^{177}Lu)-labeled aminobenzyl-DOTA [12, 14-19]. ^{177}Lu is a β -emitter (maximum energy: 0.5MeV, average energy: 0.13 MeV) with a half-life of 6.65 days, and it also emits γ -radiation that can be imaged using single-photon emission tomography (SPECT). ^{177}Lu has shown potential for radiotheranostics applications, especially for treating gastroenteropancreatic neuroendocrine tumors and metastatic castration-resistant prostate cancer [20].

Notably, three-step DOTA-PRIT based on [^{177}Lu]Lu-ABD has shown excellent therapeutic efficacy without treatment-related toxicities in subcutaneous GPA33-expressing human CRC xenograft mice [12-14, 19]. However, looking toward clinical translation, while subcutaneous xenograft tumors are easy to grow, and while their progression and response to therapeutic intervention can be easily monitored non-invasively [21, 22], the subcutaneous tumor microenvironment does not fully mirror relevant clinical situations; correspondingly, subcutaneous xenograft models are considered suboptimal models, proven to be poor predictors of drug efficacy in humans [23]. Hence, we have established an orthotopic CRC liver metastasis model using minimally invasive percutaneous ultrasound-guided intraparenchymal liver inoculation of two distinct CRC cell lines (GPA33^{high} SW1222-luc and GPA33^{low} LoVo cell lines), reflecting human CRC liver metastasis [24]. Moreover, we have also more recently developed a bivalent ^{177}Lu -based radiohaptent, [^{177}Lu]Lu-ABD-PEG₄-Lu-ABD, also referred to as [^{177}Lu]Lu-Gemini. This symmetrical dimer consists of two benzyl-DOTA radiometal chelators connected by a PEG₄ linker (**Figure 1**). This bivalent "twin" radiohaptent has shown enhanced tumor retention and improved dose delivery to tumor tissue in a subcutaneous human CRC xenograft model, while maintaining comparable renal clearance to its earlier monovalent counterpart [^{177}Lu]Lu-ABD [13, 19].

Here, our aim was to compare the efficacy and safety of bivalent vs. monovalent three-step DOTA-PRIT regimens in the orthotopic CRC liver metastasis model, to mimic a clinical path forward. The orthotopic CRC liver metastasis model is particularly relevant since patients with CRC commonly develop liver metastasis. While previous studies have relied primarily on subcutaneous xenograft models, studying treatment efficacy in the liver microenvironment itself may reveal different tumor behaviors, therapeutic responses, and potential resistance patterns that would not be apparent in subcutaneous xenograft models. Indeed, the selection of the best preclinical animal model research for the development of novel therapies is of tremendous importance, as the tumor microenvironment is known to influence the growth, treatment efficacy, and tumor immune response in vivo [21, 24]. We hypothesized that the bivalent design of [^{177}Lu]Lu-Gemini will enhance tumor uptake and retention in our orthotopic CRC liver metastasis model, potentially overcoming the limitations of monovalent radiohaptents in achieving curative tumor dose thresholds.

METHODS

Cell culture and reagents

The human CRC cell lines luciferase-transduced SW1222 (SW1222-luc, GPA33^{high}) and LoVo (GPA33^{low}) were obtained from the Memorial Sloan Kettering Cancer Center (MSK) Ludwig Institute for Cancer Immunotherapy (New York, NY, USA). According to GPA33 quantification using Quantum Simply

Cellular beads (Bangs Laboratories, Inc., Fishers, IN, USA), SW1222-luc had ~8 times higher GPA33 expression compared with LoVo (antibody binding capacity of 89023 antibodies/cell and 11342 antibodies/cell, respectively). GPA33 immunohistochemistry (IHC) confirmed these quantification findings, showing strong membranous GPA33 staining in SW1222-luc tumors compared with absent-to-low scattered GPA33 staining in LoVo tumors (**Figure S2**). Cell lines were cultured in Minimal Essential Medium (SW1222-luc) or RPMI (LoVo) supplemented with 10% heat-inactivated fetal bovine serum, 2.0 mM glutamine, 100 units/mL penicillin, and 100 units/mL streptomycin in a 37°C environment containing 5% CO₂. All media were purchased from the MSK Media Preparation Facility.

Ultrasound-guided intraparenchymal liver inoculation

All animal experiments were approved by the MSK Institutional Animal Care and Use Committee (IACUC protocol: 00-03-053). For ultrasound-guided intraparenchymal liver inoculation of SW1222-luc and LoVo cell lines, the same protocol, adapted from previous studies [24, 25], was used (**Figure S3 and Supplementary Video 1**): Athymic female nude mice *Foxn1^{nu}* (6–8 weeks old) were anesthetized with 3% (v/v) isoflurane gas in medical air at a flow rate of 3 L/min via an induction chamber, and then the mice were positioned supine on the ultrasound platform with a nose cone and maintained at 2% (v/v) isoflurane gas. Ultrasound gel was applied to their abdomens and the mice were imaged in B mode (2D) using a 40-MHz transducer (Vevo 2100, Visualsonics, Toronto, ON, Canada). A 30-gauge, half-inch needle mounted on a 25- μ L Hamilton Luer Type syringe (Model 702 LT SYR, Hamilton, Reno, NV, USA) was aligned and advanced percutaneously into the left liver freehand using the ultrasound monitor for reference. A 20- μ L suspension bolus of $\sim 1 \times 10^6$ cells/mouse in 1:1 phosphate buffer saline (PBS):Matrigel (Corning Incorporated, Corning, NY, USA) was then injected directly into the liver parenchyma at a depth of ~ 5 mm. The needle was slowly retracted immediately after the complete delivery of cells into the liver. The growth of the liver mass was evaluated weekly using the same anesthesia protocol, ultrasound machine, and ultrasound probe. The volume of the tumors was calculated by segmentation analysis of whole-body microCT scans (Inveon PET/CT, Siemens USA, Chicago, IL, USA) using VivoQuant software (Invivo, Boston, MA, USA). Approximately 80% of inoculated mice showed an adequately sized liver tumor (usually ranging from 200–900 mm³) 3 (SW1222-luc) to 4 weeks (LoVo) after intraparenchymal liver inoculation.

Three-step DOTA-PRIT reagents

The following reagents were used for three-step DOTA-PRIT: 1) An anti-GPA33/anti-DOTA IgG-scFv BsAb (molecular weight: ~ 210 kDa), produced as described previously [14, 19]; 2) a DOTA(Y)-conjugated poly-*N*-acetyl-galactosamine glycodendron clearing agent (molecular weight: 9059 Da), designed to remove circulating BsAbs rapidly by forming a complex via the DOTA(Y) moiety and clearing via liver asialogalactose receptor recognition and catabolism [16]; and 3) a choice between two radiohaptens (**Figure 1A**) – either monovalent [¹⁷⁷Lu]Lu-ABD ([¹⁷⁷Lu]Lu-S-2-(4-aminobenzyl)-1,4,7,10-tetraazacyclododecane tetraacetic acid ([¹⁷⁷Lu]Lu-ABD) or bivalent [¹⁷⁷Lu]Lu-Gemini ([¹⁷⁷Lu]Lu-ABD-PEG₄-Lu-ABD). All reagents were formulated for injection in sterile saline up to a 150- μ L volume and administered intravenously via the tail vein.

Radiosynthesis of monovalent [¹⁷⁷Lu]Lu-ABD and bivalent [¹⁷⁷Lu]Lu-Gemini

The radiopharmaceutical [¹⁷⁷Lu]LuCl₃ (no carrier added, specific activity ~ 3561 GBq/mg [623 MBq/nmol]) was supplied by Isotopia Molecular Imaging (Petah Tikva, Israel). Monovalent [¹⁷⁷Lu]Lu-ABD and bivalent [¹⁷⁷Lu]Lu-Gemini were prepared as described previously [18, 19, 26, 27]. ABD and Gemini chelated ¹⁷⁷Lu efficiently, resulting in average radiochemical conversions $> 99\%$ with a molar activity of 111 MBq/nmol and 222 MBq/nmol, respectively, and a radiochemical purity $> 98\%$ for both (see the supplementary material for further details).

Ex vivo biodistribution experiment

We conducted an ex vivo biodistribution experiment in 4 groups of mice bearing SW1222-luc tumors, to compare the monovalent [¹⁷⁷Lu]Lu-ABD and bivalent [¹⁷⁷Lu]Lu-Gemini radiohaptens in our three-step DOTA-PRIT approach. For each radiohaptent, two different pretargeting intervals (time between the BsAb and radiohaptent injections) were considered: 24 h and 48 h (**Figure 1B**). Each group (n = 20 mice) received an intravenous (i.v.) injection of anti-GPA33 BsAb (250 μ g/1.19 nmol) at either t = -24 h or -48 h, and an i.v. injection of clearing agent (25 μ g, 2.8 nmol) at t = -4 h, followed by an injection of monovalent [¹⁷⁷Lu]Lu-ABD (3.7 MBq, 0.4 nmol) or bivalent [¹⁷⁷Lu]Lu-Gemini (3.7 MBq, 0.2 nmol) at t = 0. We used half

the molar amount of bivalent [¹⁷⁷Lu]Lu-Gemini radiohapten compared with monovalent [¹⁷⁷Lu]Lu-ABD radiohapten to normalize for the number of DOTA molecules.

At designated timepoints after the radiohapten injection (2, 24, 48, and 120 h), mice (5 per time point) were euthanized humanely by CO₂ asphyxiation and ex vivo biodistribution was assessed. Tissues of interest were collected, and their activity concentration determined immediately after harvesting, using a γ-counter (Hidex Automatic Gamma Counter, Hidex Oy, Turku, Finland). Biodistribution results (**Figure 2**) were expressed as percent injected dose per gram (%ID/g) and used to estimate radiation dosimetry (see supplementary material for further details).

SPECT and quantitative autoradiography (QAR)

SW1222-luc and LoVo tumor-bearing mice were imaged with SPECT (NanoSPECT/CT, Mediso Medical Imaging Systems, Budapest, Hungary) to compare monovalent [¹⁷⁷Lu]Lu-ABD vs. bivalent [¹⁷⁷Lu]Lu-Gemini tumor targeting efficacy using an established pretargeting protocol (**Figure 1B**), with an activity of 44.4 Mbq (0.4 nmol of [¹⁷⁷Lu]Lu-ABD; 0.2 nmol of [¹⁷⁷Lu]Lu-Gemini). We used a pretargeting interval of 24h for [¹⁷⁷Lu]Lu-ABD and 48h for bivalent [¹⁷⁷Lu]Lu-Gemini. Immediately after BsAb injection, long-lasting microCT contrast (ExiTron™ nano 12000, Miltenyi Biotec, Bergisch Gladbach, Germany) was administered intravenously (100 μL) via the tail vein to enhance liver tumor visualization.

We imaged 5 SW1222-luc tumor-bearing mice with SPECT (**Figure 3**). Four mice were randomly selected from the DOTA-PRIT experiment: 2 from the [¹⁷⁷Lu]Lu-Gemini group, 1 from the [¹⁷⁷Lu]Lu-ABD group, and 1 from the control group (no BsAb injection; [¹⁷⁷Lu]Lu-ABD, 44.4 MBq, 0.4 nmol). The fifth imaged mouse received monovalent [¹⁷⁷Lu]Lu-ABD but was not part of the DOTA-PRIT experiment. All 5 mice were imaged at 24 h. Four of them were also re-imaged at 120 h: the 2 mice from the [¹⁷⁷Lu]Lu-Gemini DOTA-PRIT group, the mouse from the [¹⁷⁷Lu]Lu-ABD DOTA-PRIT group, and the mouse that received monovalent [¹⁷⁷Lu]Lu-ABD but was not included in the DOTA-PRIT experiment. Additionally, one mouse from the [¹⁷⁷Lu]Lu-ABD DOTA-PRIT group was re-imaged with SPECT at day 15 post treatment initiation, to assess tumor retargeting 24 h after the 3rd cycle of [¹⁷⁷Lu]Lu-ABD (**Figure S4**).

Of the LoVo tumor-bearing mice (n = 4) imaged with SPECT (**Figures 3 and S5**), 2 received [¹⁷⁷Lu]Lu-ABD and 2 received [¹⁷⁷Lu]Lu-Gemini. At 2 h, all 4 mice were imaged. At 24 h, the 2 [¹⁷⁷Lu]Lu-Gemini mice and 1 mouse that received [¹⁷⁷Lu]Lu-ABD were imaged. At 48 and 120 h, 1 [¹⁷⁷Lu]Lu-Gemini mouse and 1 [¹⁷⁷Lu]Lu-ABD mouse were imaged.

The counting rates in the reconstructed images were converted to mean %ID/g by applying a system-specific calibration factor for ¹⁷⁷Lu. All SPECT images were analyzed using Vivoquant software (Invicro, Boston, MA, USA).

Tumor targeting efficacy of monovalent [¹⁷⁷Lu]Lu-ABD (44.4 Mbq, 0.4 nmol, 24h pretargeting interval) vs. bivalent [¹⁷⁷Lu]Lu-Gemini (44.4 Mbq, 0.2 nmol, 48h pretargeting interval) was also assessed in 2 additional SW1222-luc tumor-bearing mice using QAR (**Figure 4**). Mice were euthanized 5 days post monovalent or bivalent radiohapten injection, and the SW1222-luc liver tumors were resected and trimmed along with some adjacent normal hepatic parenchyma for QAR analysis.

Three-step DOTA-PRIT experiment

A DOTA-PRIT experiment was performed using three groups of SW1222-luc tumor-bearing mice (n = 5 mice per group) (**Figure 5A**). The first group (“[¹⁷⁷Lu]Lu-ABD” group) underwent a monovalent [¹⁷⁷Lu]Lu-ABD treatment regimen involving three treatment cycles one week apart, with anti-GPA33 BsAb (250 μg/1.19 nmol) at t = -24 h, clearing agent (25 μg, 2.8 nmol) at t = -4 h, and monovalent [¹⁷⁷Lu]Lu-ABD (44.4 MBq, 0.4 nmol) at t = 0 h (24 h pretargeting interval). The second group (“[¹⁷⁷Lu]Lu-Gemini” group) underwent a bivalent [¹⁷⁷Lu]Lu-Gemini treatment regimen involving only a single cycle, with anti-GPA33 BsAb (250 μg/1.19 nmol) at t = -48 h, clearing agent (25 μg/2.8 nmol) at t = -4 h, and bivalent [¹⁷⁷Lu]Lu-Gemini (44.4 MBq, 0.2 nmol) at t = 0 h (48 h pretargeting interval). The third group was a control group, with all mice undergoing a multicycle treatment (three treatment cycles one week apart) of only clearing agent at t = -4h and monovalent [¹⁷⁷Lu]Lu-ABD (44.4 MBq, 0.4 nmol) at t = 0 h, without anti-GPA33 BsAb. Immediately after the BsAb injection, long-lasting microCT contrast (ExiTron™ nano 12000, Miltenyi Biotec, Bergisch Gladbach, Germany) was administered intravenously (100 μL) via the tail vein to enhance liver tumor visualization.

Periodic measurements of body weight and hematological parameters were conducted to evaluate potential signs of toxicity. Tumor progression was monitored with bioluminescence imaging (BLI) using the

IVIS Spectrum In Vivo Imaging System (PerkinElmer, Inc., Waltham, MA, USA) and microCT using the Inveon PET/CT system (Siemens USA, Chicago, IL, USA).

Mice were sacrificed if their tumor volume exceeded 1500 mm³, if they were lethargic and/or presented a distended abdomen or other significant clinical signs, or if excessive weight loss (20%) from their pretreatment baseline weight was noted. Complete or partial necropsies were performed in selected mice depending on pathology service availability, along with histopathology and GPA33 IHC. GPA33 IHC staining positivity was evaluated subjectively and graded as a percentage of positively stained cells in the tissue samples.

Data analysis

Quantitative data were expressed as mean \pm standard error of the mean (SEM) unless otherwise noted. Kaplan–Meier survival curves were analyzed using the Mantel–Cox test. For comparisons between groups, multiple Mann–Whitney U tests were performed with p-values adjusted for multiple comparisons using the two-stage step-up method of Benjamini, Krieger, and Yekutieli with a target false discovery rate (FDR) of 5%. All statistical analyses were performed using Prism 10 (GraphPad Software, San Diego, CA, USA). For all studies, a p-value less than 0.05 was considered statistically significant.

RESULTS

Ex vivo biodistribution in tumor-bearing mice and dosimetry

Both monovalent [¹⁷⁷Lu]Lu-ABD and bivalent [¹⁷⁷Lu]Lu-Gemini radiohaptens showed rapid and effective SW1222-luc tumor targeting (**Figures S6 and Table S1**). [¹⁷⁷Lu]Lu-Gemini however achieved significantly higher tumor uptake (%ID/g) compared with [¹⁷⁷Lu]Lu-ABD across all evaluated time points (2 h, 24 h, 48 h, and 120 h) for both 24 h and 48 h pretargeting intervals. There was no statistical difference in tumor uptake between the 24 h and 48 h pretargeting intervals for [¹⁷⁷Lu]Lu-Gemini, while the 24 h pretargeting interval for [¹⁷⁷Lu]Lu-ABD consistently resulted in higher tumor uptake compared with the 48 h interval at all time points (**Figure S6**).

Tumor biodistribution data of [¹⁷⁷Lu]Lu-ABD (24 h pretargeting interval) and [¹⁷⁷Lu]Lu-Gemini (48 h pretargeting interval) were analyzed using a non-linear one-phase decay curve-fitting model (**Figure 2C**), with successful fitting of both curves ($R^2 = 0.91$ for [¹⁷⁷Lu]Lu-ABD, and 0.86 for [¹⁷⁷Lu]Lu-Gemini). The analysis confirmed the superior tumor retention of [¹⁷⁷Lu]Lu-Gemini (48 h pretargeting) compared with [¹⁷⁷Lu]Lu-ABD (24 h pretargeting), with a tumor biological half-life and plateau of respectively 13.4 h and 1.3 %ID/g for [¹⁷⁷Lu]Lu-ABD, and 25.4 h and 4.5 %ID/g for [¹⁷⁷Lu]Lu-Gemini. The extended biological tumor half-life of [¹⁷⁷Lu]Lu-Gemini better complemented lutetium-177 physical half-life (6.7 days), while its elevated plateau provided a 3.5-fold increase in sustained tumor activity compared to [¹⁷⁷Lu]Lu-ABD - both characteristics having the potential of significantly improving the therapeutic efficacy of [¹⁷⁷Lu]Lu-Gemini.

Mean absorbed doses for tumor and normal tissues (**Table 1**) were estimated for both radiohaptens based on ex vivo biodistribution results (**Table S1**), to help guide our DOTA-PRIT experiment and predict dose-limiting tissues. The therapeutic index (TI) values, representing the ratio between the tumor and the respective normal tissue mean absorbed doses were also calculated, with higher TI values indicating better therapeutic efficacy with potentially fewer side effects. For 24 h pretargeting interval [¹⁷⁷Lu]Lu-ABD, the mean absorbed doses (in cGy/MBq) and TI were as follows: tumor 32.88, blood 2.14 (TI = 15), normal liver 3.14 (TI = 10), and kidneys 6.94 (TI = 5). In comparison, 48 h pretargeting interval [¹⁷⁷Lu]Lu-Gemini showed higher mean absorbed doses (in cGy/MBq): 119.88 for tumor, 2.40 for blood (TI = 50), 5.85 for normal liver (TI = 20), and 13.23 for kidneys (TI = 9). Based on these estimates, [¹⁷⁷Lu]Lu-Gemini PRIT would deliver a significantly higher mean absorbed dose to the tumor (by a factor of ~4) and achieve more favorable TIs compared with monovalent [¹⁷⁷Lu]Lu-ABD PRIT across the evaluated tissues. For both radiohaptens, the kidneys would receive the highest dose compared with other organs.

When considering the administered activity per cycle in our DOTA-PRIT experiment (44.4 MBq), both [¹⁷⁷Lu]Lu-ABD and [¹⁷⁷Lu]Lu-Gemini treatment regimens would lead to significant tumor responses (estimated cumulative absorbed dose delivered to the tumor: 44 Gy for the [¹⁷⁷Lu]Lu-ABD treatment regimen (three cycles) and 53 Gy for the [¹⁷⁷Lu]Lu-Gemini treatment regimen (single cycle)) while maintaining kidney doses below the currently accepted normal tissue dose limit and toxicity endpoint of 23–26 Gy for radiopharmaceutical therapy [28] (projected cumulative doses of 9.2 Gy for the [¹⁷⁷Lu]Lu-ABD treatment regimen (three cycles) and 5.9 Gy for the [¹⁷⁷Lu]Lu-Gemini treatment regimen (single cycle)). This tumor dose comparison underscores the tremendous advantage of the single-cycle [¹⁷⁷Lu]Lu-Gemini

treatment regimen which allows, with just one administration, the delivery of an estimated tumor dose surpassing the cumulative dose achieved by the [¹⁷⁷Lu]Lu-ABD treatment regimen over three treatment cycles.

Using the activity concentration in the blood as a surrogate for bone marrow activity concentration, our estimates also indicate that the mean absorbed dose to the bone marrow, considered the most radiosensitive organ, would remain below the threshold of 2.5 Gy for the [¹⁷⁷Lu]Lu-Gemini treatment regimen (1.1 Gy), while this threshold would be reached after three treatment cycles of the [¹⁷⁷Lu]Lu-ABD treatment regimen (2.8 Gy over three cycles) [28]. It is, however, important to note that the bone marrow can regenerate to some extent during multicycle treatments, allowing for potential retreatment without the need for extended recovery periods, unlike slower regenerating organs such as the liver or kidneys, where radiation effects are viewed as cumulative and additive toward an upper limit [28].

SPECT and QAR results

SPECT results at 24 h showed efficient tumor targeting by both [¹⁷⁷Lu]Lu-ABD and [¹⁷⁷Lu]Lu-Gemini for SW1222-luc tumors (**Figure 3**). With [¹⁷⁷Lu]Lu-ABD, the tumor uptake was 5.39 ± 1.34 %ID/g ($n = 2$), and the tumor-to-normal tissue (T:NT) ratios were 15.8 (kidneys) and 45.9 (blood). With [¹⁷⁷Lu]Lu-Gemini, the tumor uptake was 15.23 ± 2.46 %ID/g ($n = 2$), and the T:NT ratios were 23.7 (kidneys) and 61.0 (blood). Meanwhile, at this same timepoint, negligible tumor targeting, with a tumor uptake of 0.07 %ID/g (image not shown), was observed in the imaged control mouse. Of note, at 5 days, follow-up SPECT (**Figure 3**) and QAR (**Figure 4**) showed superior tumor retention of [¹⁷⁷Lu]Lu-Gemini (9.44 ± 1.00 %ID/g, $n = 2$, on SPECT analysis) compared to [¹⁷⁷Lu]Lu-ABD (1.76 %ID/g, $n = 1$, on SPECT analysis). Efficient tumor retargeting after the 3rd cycle of [¹⁷⁷Lu]Lu-ABD was also confirmed on SPECT (**Figure S4**), with a tumor uptake of 6.95 %ID/g at 24 h.

The observed discrepancies in SW1222-luc tumor uptake values between the ex vivo biodistribution experiment and SPECT imaging (for instance, 9.62 ± 0.55 %ID/g ($n = 5$) at 24 h for [¹⁷⁷Lu]Lu-Gemini in the ex vivo biodistribution experiment, versus 15.23 ± 2.46 %ID/g ($n = 2$) with SPECT imaging) could be attributed to several factors. Firstly, the smaller SPECT imaging sample size likely played an important role, with a notable individual variation in tumor uptake, as demonstrated by the high SEM on the SPECT images compared with the ex vivo biodistribution experiment. Secondly, the quantification could be affected by the inherent methodological variations between the two techniques and how regions of interest (ROIs) are defined and analyzed on SPECT images for %ID/g calculations versus direct tissue measurements in the ex vivo biodistribution experiment.

Finally, SPECT results at 24 h showed superior tumor targeting by [¹⁷⁷Lu]Lu-Gemini compared with [¹⁷⁷Lu]Lu-ABD for low GPA33-positive LoVo tumors (**Figures 3 and S5**). With [¹⁷⁷Lu]Lu-Gemini, the tumor uptake was 2.91 ± 0.23 %ID/g ($n = 2$), and the T:NT ratios were 4.4 (kidneys) and 6.7 (blood). In contrast, with [¹⁷⁷Lu]Lu-ABD, the tumor uptake was minimal at only 0.57 %ID/g ($n = 1$), and the T:NT ratios were 1.0 (kidneys) and 3.4 (blood). At 120 h, LoVo tumor uptake remained relatively unchanged for both radiohaptenes. With [¹⁷⁷Lu]Lu-Gemini, the tumor uptake was 2.69 %ID/g ($n = 1$), with minimally improved T:NT ratios (5.8 for kidneys, 10 for blood). With [¹⁷⁷Lu]Lu-ABD, the tumor uptake remained minimal at 0.45 %ID/g ($n = 1$), and the T:NT ratios were 1.8 (kidneys) and 3.3 (blood).

DOTA-PRIT experiment results

The liver tumor response curves (CT and BLI) for treatment and control (i.e., clearing agent and [¹⁷⁷Lu]Lu-ABD but no BsAb) groups are shown in **Figures 5 and S7**. In the control group, rapid tumor progression above the experiment endpoint (> 1500 mm³) was observed, leading to the euthanasia of all mice ($n = 5$) by day 18. In [¹⁷⁷Lu]Lu-ABD and [¹⁷⁷Lu]Lu-Gemini treatment groups, the liver tumors continued to grow for 2–3 weeks after the initiation of the 1st treatment cycle, before decreasing in size and BLI signal, reaching a nadir at ~45 days (**Figures 5 and S7**). At this timepoint, only residual liver tumors/scar tissue surrounded by a rim of contrast medium were visible on CT (**Figure 5C**). Liver tumor size decreased from 153 ± 92 mm³ at D₀ to 18 ± 8 mm³ at D₄₄ for the [¹⁷⁷Lu]Lu-ABD group ($n = 2$ mice imaged), and from 434 ± 174 mm³ to 60 ± 20 mm³ for the [¹⁷⁷Lu]Lu-Gemini group ($n = 5$ mice imaged). 3/5 mice from the [¹⁷⁷Lu]Lu-ABD group had perivenous extravasation of contrast medium (visible on CT, not shown), which prevented the evaluation of their liver tumor size on CT. To minimize additional handling of the treated mice, a second injection of contrast medium was not attempted. Injecting the contrast medium at a separate timepoint ($t = -72$ h for instance) rather than immediately after the BsAb could prevent this issue and should be considered in future studies. On BLI, the total photon flux decreased 10-fold for both treatment groups, from

$2.97 \times 10^9 \pm 1.56 \times 10^9$ photons/s at D₀ to $2.95 \times 10^8 \pm 1.18 \times 10^8$ photons/s at D₄₄ for the [¹⁷⁷Lu]Lu-ABD group (n = 5 mice imaged), and from $1.41 \times 10^9 \pm 4.46 \times 10^8$ photons/s to $1.56 \times 10^8 \pm 5.77 \times 10^7$ photons/s for the [¹⁷⁷Lu]Lu-Gemini group (n = 5 mice imaged). Treatments were well tolerated, without significant weight loss or hematologic changes between groups or deviation from reference ranges (**Figure S8**).

Eventually, all mice from the treatment groups met one of the experiment endpoint criteria, requiring euthanasia. For the three [¹⁷⁷Lu]Lu-ABD-treated mice with contrast medium perivenous extravasation and for the control mice that did not receive contrast medium, the decision to euthanize was taken when significant abdominal distension/tumor burden was detected on abdominal palpation (tumors reaching a diameter of ~1.4 cm, corresponding to an approximate volume of 1500 mm³). The median survival time (**Figure 5D**) was 18 days for the control group, 71 days for the [¹⁷⁷Lu]Lu-ABD group, and 81 days for the [¹⁷⁷Lu]Lu-Gemini group – with survival time being statistically different between treatment and control groups (p < 0.01, logrank Mantel–Cox), but not between treatment groups (p = 0.53, log-rank Mantel–Cox).

Toxicity assessment

At the time of death, 8/10 treated mice exhibited large recurrent liver tumors exceeding the experiment endpoint size (1500 mm³), requiring euthanasia. Necropsies were performed on 7/10 treated mice, some undergoing complete examinations (5/7 necropsied mice), and others partial necropsies (2/7 necropsied mice), limited to the liver, kidneys, and femur/bone marrow (**Table S2**), depending on pathology service availability. Histopathological examination revealed large liver adenocarcinomas consistent with SW1222-luc xenograft implantation in 5/7 necropsied treated mice, often with metastases to abdominal structures, and in one case, to the lungs. Two treated mice demonstrated distinct outcomes, i.e., not presenting with a distended abdomen and/or a recurrent liver mass (**Figure S9**). One [¹⁷⁷Lu]Lu-Gemini-treated mouse (G2M4 mouse in **Table 2**) had complete liver tumor regression, with only scar tissue identified histologically at the inoculation site, consistent with complete response to treatment (**Figure S9A–C**). This mouse, however, developed a head tilt at day 81, requiring euthanasia. There was no detectable neoplasia in the tissues submitted for histology (limited to liver, kidneys, and femur/bone marrow), but a full necropsy was not performed, and the possibility of a distant metastasis could therefore not be excluded (**Table S2**). Another [¹⁷⁷Lu]Lu-Gemini-treated mouse (G2M5 mouse in **Table 2**), euthanized for acute hindlimb paralysis on day 68, had a residual liver tumor mostly composed of fibrosis, necrotic debris, mucin, and granulomatous inflammation, with only few viable tumor cells (**Figure S9D–G**). This mouse also developed a large highly cellular spinal cord metastasis, leading to euthanasia (**Figure S9H–K**).

Necropsies (2 complete and 3 partial) were also performed on control mice. A consistent histological finding among treated mice compared with control mice was marked ovarian atrophy (**Table S2**), absent in control mice, aligning with previous studies and interpreted as a treatment-related effect [19, 29, 30]. No significant microscopic change indicative of treatment-related radiotoxicity was observed in the kidneys, urinary bladder, liver, spleen, or bone marrow. One [¹⁷⁷Lu]Lu-Gemini-treated mouse displayed moderate chronic cholangiohepatitis and occasional foci of hepatocyte necrosis, but similar liver necrosis was observed in control mice and was therefore attributed to the large liver tumors rather than related to treatment. Additional microscopic findings (**Table S2**) were considered incidental or typical background changes for the mouse strain, sex, and age, and were not interpreted as treatment-related effects [31].

GPA33 IHC

GPA33 immunostaining was performed on the recurrent liver tumors from 5 treated mice, the liver of the 2 treated mice without a recurrent liver tumor, and the liver from 1 control mouse (**Figure S9**). In addition, GPA33 immunostaining was also performed on 6 extrahepatic metastatic lesions (pancreas, small intestine, spinal cord, mesometrium, axillary lymph node, and diaphragm) from 3 treated mice (2 from the [¹⁷⁷Lu]Lu-Gemini group and 1 from the [¹⁷⁷Lu]Lu-ABD group) (**Table 2 and Figure S10**). Among the 12 viable tumor samples from treated mice (excluding the liver of the mouse with only scar tissue (G2M4 in **Table 2**)), 83% (10/12) demonstrated high GPA33 cell positivity, with over 70% of tumor cells staining positively (**Table 2 and Figure S10A–G**). However, 17% (2/12) of the samples had less than 20% positively stained tumor cells (**Figure 6, Figure S9H–K, and Table 2**), suggesting the possibility of immune tumor evasion and/or loss of GPA33 antigen/epitope expression in these samples. Strong GPA33 IHC signal positivity was present in the liver tumor of the control mouse (image not shown).

DISCUSSION

This study demonstrates the considerable potential of three-step DOTA-PRIT to treat CRC liver metastases, particularly three-step DOTA-PRIT based on the bivalent [¹⁷⁷Lu]Lu-Gemini radiohapten, as demonstrated in an orthotopic CRC liver metastasis model. Tumor response to DOTA-PRIT was assessed using a combination of sequential CT scans and BLI in five mice that underwent the monovalent [¹⁷⁷Lu]Lu-ABD treatment regimen (three weekly treatment cycles), five mice that underwent the bivalent [¹⁷⁷Lu]Lu-Gemini treatment regimen (single-cycle treatment), and five control mice that received monovalent [¹⁷⁷Lu]Lu-ABD but did not have any BsAb injection. The control group had the lowest median survival of 18 days, with progressive increase tumor size requiring sacrifice of all control mice by day 18. In comparison, both the [¹⁷⁷Lu]Lu-ABD and [¹⁷⁷Lu]Lu-Gemini treatment regimens resulted in remarkable SW1222-luc tumor targeting efficacy, which ultimately led to a 4-fold increase in survival compared with control group, without evidence of acute toxicity. Of note, median survival was similar for mice treated with multicycle [¹⁷⁷Lu]Lu-ABD (71 days) and those treated with single-cycle [¹⁷⁷Lu]Lu-Gemini (81 days).

For our DOTA-PRIT experiment, the pretargeting interval for each radiohapten was selected based on previous publications [19, 27, 32] and the results of our ex vivo biodistribution experiment. For [¹⁷⁷Lu]Lu-ABD, using a 24 h pretargeting interval was justified by the consistently higher tumor uptake at all time points compared to the 48 h pretargeting interval (**Figure S6**), along with favorable TI (**Table 1**) for all examined organs. For [¹⁷⁷Lu]Lu-Gemini, although tumor, kidney or blood uptake did not show statistically significant differences between the two pretargeting intervals (**Figure S6**), we chose the 48 h interval because of its improved TI (**Table 1**), and to align with recent studies in which longer intervals (up to 3 days) have been used to optimize tumor targeting and blood clearance [13, 29, 33]. Using these pretargeting intervals, comparable radiation doses to tumors were also achieved with both radiohaptens: 44 Gy for 3 therapy cycles of 44.4 Mbq of [¹⁷⁷Lu]Lu-ABD, and 53 Gy for a single cycle of 44.4 Mbq of [¹⁷⁷Lu]Lu-Gemini, allowing adequate therapeutic efficacy comparison of the two platforms.

Both treatment regimens maintained high TIs for blood and kidney, with [¹⁷⁷Lu]Lu-Gemini exhibiting superior performance by delivering a mean absorbed dose to the tumor almost four times higher compared with [¹⁷⁷Lu]Lu-ABD and achieving more favorable therapeutic indices across the evaluated tissues (**Table 1**). Finally, a maximum tolerated dose was not reached for either treatment regimen.

The advantages of the [¹⁷⁷Lu]Lu-Gemini over the [¹⁷⁷Lu]Lu-ABD were even more noticeable in low GPA33-positive LoVo tumors. In these tumors, the tumor uptake of [¹⁷⁷Lu]Lu-Gemini on SPECT images acquired 24 h and 120 h post injection was clearly higher than that of [¹⁷⁷Lu]Lu-ABD ([¹⁷⁷Lu]Lu-Gemini: 2.91 ± 0.32 %ID/g (n = 2) and 2.69 %ID/g (n = 1) at 24 h and 120 h, respectively; [¹⁷⁷Lu]Lu-ABD: 0.57 %ID/g (n = 1) and 0.45 %ID/g for ABD (n = 1), at 24 h and 120 h, respectively). These results confirmed the superiority of the [¹⁷⁷Lu]Lu-Gemini treatment regimen over the [¹⁷⁷Lu]Lu-ABD treatment regimen, which is attributed to [¹⁷⁷Lu]Lu-Gemini's dual binding feature and higher tumoral retention over time. This finding could have a tremendous clinical impact: by allowing similar or even higher tumor targeting while decreasing the number of drug injections, patients' treatment burden can be improved. On the other hand, the increased renal uptake observed with [¹⁷⁷Lu]Lu-Gemini warrants careful consideration for future clinical translation, especially if multicycle [¹⁷⁷Lu]Lu-Gemini treatments will be considered. Similarly, even though our dosimetry estimates indicate that a single dose of [¹⁷⁷Lu]Lu-Gemini would keep the bone marrow mean absorbed dose (1.1 Gy) below the accepted dose limit of 2–3 Gy, multicycle [¹⁷⁷Lu]Lu-Gemini treatments could significantly increase this dose, requiring careful monitoring for hematological toxicity.

Our GPA33 IHC results highlight important considerations for three-step DOTA-PRIT clinical application. While most recurrent liver tumors and extrahepatic metastases (i.e., metastases beyond the liver) maintained high GPA33 expression post-treatment, a small subset (17%, 2/12) of submitted samples showed less than 20% positively stained tumor cells (**Figures 6 and S9**). This result suggests possible immune tumor evasion and/or loss of GPA33 antigen/epitope expression. Potential mechanisms may include the removal of antigens from the cell surface (via internalization or trogocytosis), disrupted trafficking to the cell membrane, transcriptional downregulation, or genomic alterations [34, 35]. A reduction in the average expression of the targeted antigen after treatment could also occur due to the elimination of tumor cell subpopulations with the highest antigen levels [34, 35]. This finding emphasizes the importance of the theranostic concept, i.e., the necessity of conducting immunoPET with a suitable companion PET agent before considering PRIT (in our three-step DOTA-PRIT approach, for instance, the β⁺ isotope yttrium-86 could be used as an imaging surrogate for lutetium-177). Finally, this finding accentuates the potential benefits of multivalent antigen targeting, either simultaneously or sequentially, and the selection of different

antigen combinations (depending on antigen density differences across tumors) to overcome tumor treatment escape.

Our current orthotopic CRC liver SW1222-luc metastasis model complements previous DOTA-PRIT results obtained with a subcutaneous SW1222 xenograft model [19]. While both models confirmed the superiority of [¹⁷⁷Lu]Lu-Gemini over [¹⁷⁷Lu]Lu-ABD, there were notable differences in tumor ex vivo biodistribution results and therapy outcomes. In the biodistribution experiment, [¹⁷⁷Lu]Lu-Gemini tumor %ID/g was higher in the subcutaneous model compared with the orthotopic liver model. For instance, at 2 h [¹⁷⁷Lu]Lu-Gemini (48 h pretargeting) tumor uptake was 29.5 ± 6.0 %ID/g (mean \pm SD, n= 4) in the subcutaneous model and 14.0 ± 1.9 %ID/g (mean \pm SD, n= 5) in the liver model. At 120 h, it was 16.7 ± 3.0 %ID/g (mean \pm SD, n= 4) in the subcutaneous model and 4.9 ± 0.7 %ID/g (mean \pm SD, n= 5) in the orthotopic liver model. This led to much higher estimated mean absorbed doses to the tumor and TI in the subcutaneous model: 455 cGy/MBq for [¹⁷⁷Lu]Lu-Gemini and 69.79 cGy/MBq for [¹⁷⁷Lu]Lu-ABD, versus 119.88 cGy/MBq for [¹⁷⁷Lu]Lu-Gemini and 32.88 cGy/MBq for [¹⁷⁷Lu]Lu-ABD in the orthotopic liver model. [¹⁷⁷Lu]Lu-Gemini therapy in the subcutaneous model also achieved 100% complete response with 40% histologic cure using a single 44.4 MBq treatment, while all treated mice in the orthotopic liver model developed a recurring liver mass and/or metastatic disease ultimately requiring euthanasia. The tumor microenvironment and metastatic potential of the hepatic tumors likely influenced therapeutic agent accessibility and radiation response, which could partially explain these differences. The survival difference between the 2 models may also relate to the shorter duration of the subcutaneous model experiment (80 days, versus 128 days for our current liver model). One of the most significant differences that also likely contributed to this survival discrepancy was the CRC extrahepatic dissemination in the orthotopic liver model (**Table S2**), which was absent in the subcutaneous model, where tumors remained confined to the injection site [19]. While this could be due to true hematogenous metastatic dissemination related to hepatic tumor localization, it may also have resulted from inadvertent direct hematogenous systemic seeding into the hepatic venous circulation at the time of inoculation. This assumption is supported by the presence of extrahepatic CRC dissemination (**Table S2**: right ventricle, lungs, abdominal wall, mesometrium) in 2 fully necropsied control mice, despite their short survival time (11 and 18 days). Because of the small size of the mouse liver and dense parenchymal vascularization, such dissemination may however be difficult to avoid. To prevent extrahepatic cell migration, we have refined our current ultrasound-guided intraparenchymal liver inoculation protocol, to inject even smaller inoculation volumes (~10 μ L, 2–3 million cells) in 100% Matrigel.

In our PRIT experiment, marked ovarian atrophy was observed in both therapy groups, aligning with our previous preclinical [¹⁷⁷Lu]Lu-PRIT results [19, 29, 30] and suggesting radiation-induced damage to germ cells. The close anatomical proximity of the ovaries to the kidneys in mice compared to humans, along with their distinct body size and conformation, could have also contributed to the ovarian atrophy observed in our PRIT preclinical models. While the estimated median lethal dose (LD50) for ovarian follicles is 4 Gy in humans [36, 37], a dose higher than 20 Gy in women below 40 years of age and 6 Gy in older women is required to induce permanent ovarian failure [28, 36, 38, 39] and our estimated doses to the ovaries remained way below these critical thresholds (1.6 Gy for a single therapy cycle of [¹⁷⁷Lu]Lu-Gemini and 3.0 Gy for 3 cycles of [¹⁷⁷Lu]Lu-ABD). Unlike ovaries where the main concern is sterilization, uterine radiation damage is linked to a functional capacity for pregnancy and specific dose limits are not as confidently established. A uterine radiation dose below 4 Gy should however not impair pregnancy function [40]. In our study, the [¹⁷⁷Lu]Lu-ABD cumulative dose (5.4 Gy for 3 therapy cycles) slightly exceeded this level, while [¹⁷⁷Lu]Lu-Gemini (2.7 Gy) fell below it. Nevertheless, both estimated doses remained well under the suggested critical thresholds for pregnancy concerns (uterine dose >45 Gy during adulthood and >25 Gy in childhood [40]), inferring that both PRIT platforms should preserve uterine functional capacity for pregnancy. These findings however warrant further investigation and highlight the importance of comprehensive reproductive toxicity assessment when developing radiopharmaceutical therapies.

One of the major limitations of our current 3-step DOTA-PRIT regimen is the necessity of a clearing agent to remove unbound BsAbs. To address this, we have recently established a 2-step approach alleviating the need for clearing agent, by engineering a dual scFv bispecific platform (anti-GPA33/anti-DOTA) fused to a human p53 tetramerization (p53_{tet})-based self-assembling and disassembling (SADA) domain [33, 41]. Efforts are currently ongoing to combine this SADA BsAb platform with [¹⁷⁷Lu]Lu-Gemini. Preliminary investigation of [¹⁷⁷Lu]Lu-Gemini in a subcutaneous xenograft model has shown promising results [33], and we have also successfully established a pretargeting PET approach using [⁸⁶Y]Y-Gemini as an imaging surrogate of [¹⁷⁷Lu]Lu-Gemini (unpublished data). Upcoming studies are currently in progress

to evaluate the [¹⁷⁷Lu]Lu-Gemini SADA-based PRIT and PET approach in our orthotopic CRC liver metastasis model.

CONCLUSIONS

Three-step DOTA-PRIT, particularly three-step DOTA-PRIT based on the bivalent [¹⁷⁷Lu]Lu-Gemini radiohapten, was effective in treating CRC liver metastasis in an orthotopic CRC liver metastasis model. Both monovalent and bivalent three-step DOTA-PRIT regimens increased the median survival 4-fold compared with controls and did not exert any acute toxicity. Notably, tumor dose efficiency was markedly enhanced with the bivalent [¹⁷⁷Lu]Lu-Gemini system, which delivered an estimated mean absorbed dose to the tumor of 53 Gy in a single cycle (119.88 cGy/MBq), exceeding the 44 Gy cumulative absorbed dose achieved through three therapy cycles of [¹⁷⁷Lu]Lu-ABD (32.88 cGy/MBq per cycle). The enhanced tumor uptake and retention of bivalent [¹⁷⁷Lu]Lu-Gemini could therefore be of tremendous benefit in the clinic. Our results also highlight the importance of a theranostic approach and the potential need for multivalent targeting strategies to address tumor heterogeneity and the possible loss of tumor antigen/selective tumoral cells subpopulation during serial treatments.

ABBREVIATIONS

ABD: aminobenzyl-DOTA; AUC: area under the curve; BLI: bioluminescence imaging; BsAb: bispecific antibody; CRC: colorectal cancer; CT: computed tomography; DOTA: 1,4,7,10-tetraazacyclododecane-1,4,7,10-tetraacetic acid; FDR: false discovery rate; GPA33: glycoprotein A33; H&E: hematoxylin and eosin; IHC: immunohistochemistry; IgG: immunoglobulin G; LD50: median lethal dose; MEM: minimal essential medium; MIP: maximum intensity projection; MPR: multiplanar reconstruction; MSK: Memorial Sloan Kettering Cancer Center; OCT: optimal cutting temperature; PBS: phosphate-buffered saline; PET: positron emission tomography; PRIT: pretargeted radioimmunotherapy; QAR: quantitative autoradiography; ROI: region-of-interest; SADA: self-assembling-disassembling antibody platform; scFv: single-chain fragment variable; SD: standard deviation; SEM: standard error of the mean; SPECT: single-photon emission computed tomography; TI: therapeutic index; %ID/g: percent injected dose per gram; T:NT: tumor-to-normal tissue ratio.

Acknowledgments

This research was funded in part by the Hedvig Hricak Chair in Radiology (to S.M.L.), Enid A. Haupt Chair (to N.K.C.), Center for Targeted Radioimmunotherapy and Theranostics, Ludwig Center for Cancer Immunotherapy of MSK (to S.M.L.), and Mr. William H. Goodwin and Mrs. Alice Goodwin and the Commonwealth Foundation for Cancer Research and the Experimental Therapeutics Center of MSK (to S.M.L.). S.M.C. was also supported in part by NIH/NCI P50 CA86438. This study also received support from NIH/NCI R01 CA233896 (to S.M.C.). We also acknowledge NIH/NCI cancer center support grant P30 CA008748 for use of the Tri-Institutional Laboratory of Comparative Pathology of MSK, Weill Cornell Medicine, and Rockefeller University; technical services provided by the MSK Small Animal Imaging Core Facility and Laboratory of Comparative Pathology; and the Molecular Cytology Core Facility. Funding for the Organic Synthesis Core is provided through the NIH/NCI P30 CA008748 and NCI R50 CA243895 (to O.O.). We would like to thank Dr. Kimon Argyropoulos for the review of the GPA33 IHC slides, and Joanne Chin and Leah Bassity for editing the manuscript. We gratefully acknowledge Hamilton for providing syringes through their Syringe Grant award (February 2022).

Competing Interests

Both MSK and N.K.C. have financial interest in Y-mAbs Therapeutics, Inc., Abpro-Labs, and Lallemand-Biotec Pharmacon. N.K.C. reports receiving commercial research grants from Y-mAbs Therapeutics, Inc. and Abpro-Labs. N.K.C. was named as inventor on multiple patents filed by MSK, including those licensed to Y-mAbs Therapeutics, Inc., Lallemand-Biotec Pharmacon, and Abpro-Labs. N.K.C. is a scientific advisory board member for Eureka Therapeutics. N.K.C., S.M.L., S.M.C., D.R.V., O.O., E.K.F., G.Y., and H.X. were named as inventors on some or all the following patent applications related to GPA33: SK2014-074, SK2015-091, SK2017-079, SK2018-045, SK2014-116, SK2016-052, and SK2018-068 filed by MSK. S.M.L. reports receiving commercial research grants from Genentech, Inc., WILEX AG, Telix Pharmaceuticals Limited, and Regeneron Pharmaceuticals, Inc.; holding ownership interest/equity in Elucida Oncology, Inc. and Y-mAbs Therapeutics, Inc.; and holding stock in ImaginAb, Inc. S.M.L. is the inventor and owner of issued patents both currently unlicensed and licensed by MSK to Samus

Therapeutics, Inc., Elucida Oncology, Inc., and Y-mAbs Therapeutics, Inc.. S.M.L serves or has served as a consultant to Cynvec LLC, Eli Lilly & Co., Prescient Therapeutics Limited, Advanced Innovative Partners, LLC, Gerson Lehrman Group, Progenics Pharmaceuticals, Inc., and Janssen Pharmaceuticals, Inc. G.Y. and O.O. are listed as inventors and receive royalties from patents that were filed by MSK. O.O. is an unpaid member of the scientific advisory board of Angiogenex and owns shares in Angiogenex. D.R.V. is an inventor on intellectual property licensed to ORIC Pharmaceuticals. A.C. reports receiving research funding from GSK, Seagen, and Inspirna, and is a member of the advisory board of Bayer, GSK, Merck, Janssen, G1 Therapeutics, and Seagen. All other authors have no competing interests.

REFERENCES

1. Simon K. Colorectal cancer development and advances in screening. *Clin Interv Aging*. 2016; 11: 967-76.
2. Marmol I, Sanchez-de-Diego C, Pradilla Dieste A, Cerrada E, Rodriguez Yoldi MJ. Colorectal Carcinoma: A General Overview and Future Perspectives in Colorectal Cancer. *Int J Mol Sci*. 2017; 18.
3. Brown KGM, Solomon MJ, Mahon K, O'Shannassy S. Management of colorectal cancer. *BMJ*. 2019; 366: l4561.
4. Riihimaki M, Hemminki A, Sundquist J, Hemminki K. Patterns of metastasis in colon and rectal cancer. *Sci Rep*. 2016; 6: 29765.
5. Biller LH, Schrag D. Diagnosis and Treatment of Metastatic Colorectal Cancer: A Review. *JAMA*. 2021; 325: 669-85.
6. Elferink MA, de Jong KP, Klaase JM, Siemerink EJ, de Wilt JH. Metachronous metastases from colorectal cancer: a population-based study in North-East Netherlands. *Int J Colorectal Dis*. 2015; 30: 205-12.
7. Sanchez-Gundin J, Fernandez-Carballido AM, Martinez-Valdivieso L, Barreda-Hernandez D, Torres-Suarez AI. New Trends in the Therapeutic Approach to Metastatic Colorectal Cancer. *Int J Med Sci*. 2018; 15: 659-65.
8. Crooke H, Kobayashi M, Mitchell B, Nwokeji E, Laurie M, Kamble S, et al. Estimating 1- and 5-year relative survival trends in colorectal cancer (CRC) in the United States: 2004 to 2014. *Journal of Clinical Oncology*. 2018; 36: 587-.
9. Cheal SM, Chung SK, Vaughn BA, Cheung NV, Larson SM. Pretargeting: A Path Forward for Radioimmunotherapy. *J Nucl Med*. 2022; 63: 1302-15.
10. Carrasquillo JA, Pandit-Taskar N, O'Donoghue JA, Humm JL, Zanzonico P, Smith-Jones PM, et al. (124)I-huA33 antibody PET of colorectal cancer. *J Nucl Med*. 2011; 52: 1173-80.
11. Sakamoto J, Kojima H, Kato J, Hamashima H, Suzuki H. Organ-specific expression of the intestinal epithelium-related antigen A33, a cell surface target for antibody-based imaging and treatment in gastrointestinal cancer. *Cancer Chemother Pharmacol*. 2000; 46 Suppl: S27-32.
12. Cheal SM, Fung EK, Patel M, Xu H, Guo HF, Zanzonico PB, et al. Curative Multicycle Radioimmunotherapy Monitored by Quantitative SPECT/CT-Based Theranostics, Using Bispecific Antibody Pretargeting Strategy in Colorectal Cancer. *J Nucl Med*. 2017; 58: 1735-42.
13. Vaughn B, Veach D, Burnes Vargas D, Seo S, Punzalan B, Zanzonico P, et al. Establishment of efficacy of DOTA-based pretargeted radioimmunotherapy with a bivalent radiohapten for enhanced therapeutic indices. *J Nucl Med*. 2022; 63: 2881.
14. Cheal SM, Xu H, Guo HF, Lee SG, Punzalan B, Chalasani S, et al. Theranostic pretargeted radioimmunotherapy of colorectal cancer xenografts in mice using picomolar affinity 86Y- or 177Lu-DOTA-Bn binding scFv C825/GPA33 IgG bispecific immunoconjugates. *Eur J Nucl Med Mol Imaging*. 2016; 43: 925-37.
15. Cheal SM, McDevitt MR, Santich BH, Patel M, Yang G, Fung EK, et al. Alpha radioimmunotherapy using (225)Ac-proteus-DOTA for solid tumors - safety at curative doses. *Theranostics*. 2020; 10: 11359-75.
16. Cheal SM, Patel M, Yang G, Veach D, Xu H, Guo HF, et al. An N-Acetylgalactosamino Dendron-Clearing Agent for High-Therapeutic-Index DOTA-Hapten Pretargeted Radioimmunotherapy. *Bioconjug Chem*. 2020; 31: 501-6.
17. Cheal SM, Xu H, Guo HF, Patel M, Punzalan B, Fung EK, et al. Theranostic pretargeted radioimmunotherapy of internalizing solid tumor antigens in human tumor xenografts in mice: Curative treatment of HER2-positive breast carcinoma. *Theranostics*. 2018; 8: 5106-25.

18. Cheal SM, Xu H, Guo HF, Zanzonico PB, Larson SM, Cheung NK. Preclinical evaluation of multistep targeting of diasialoganglioside GD2 using an IgG-scFv bispecific antibody with high affinity for GD2 and DOTA metal complex. *Mol Cancer Ther.* 2014; 13: 1803-12.
19. Vaughn BA, Lee SG, Vargas DB, Seo S, Rinne SS, Xu H, et al. Theranostic GPA33-Pretargeted Radioimmunotherapy of Human Colorectal Carcinoma with a Bivalent (¹⁷⁷Lu)-Labeled Radiohaptent. *J Nucl Med.* 2024.
20. Bodei L, Herrmann K, Schoder H, Scott AM, Lewis JS. Radiotheranostics in oncology: current challenges and emerging opportunities. *Nat Rev Clin Oncol.* 2022; 19: 534-50.
21. Lavilla-Alonso S, Abo-Ramadan U, Halavaara J, Escutenaire S, Tatlisumak T, Saksela K, et al. Optimized mouse model for the imaging of tumor metastasis upon experimental therapy. *PLoS One.* 2011; 6: e26810.
22. Ramasawmy R, Johnson SP, Roberts TA, Stuckey DJ, David AL, Pedley RB, et al. Monitoring the Growth of an Orthotopic Tumour Xenograft Model: Multi-Modal Imaging Assessment with Benchtop MRI (1T), High-Field MRI (9.4T), Ultrasound and Bioluminescence. *PLoS One.* 2016; 11: e0156162.
23. Sharpless NE, Depinho RA. The mighty mouse: genetically engineered mouse models in cancer drug development. *Nat Rev Drug Discov.* 2006; 5: 741-54.
24. McVeigh LE, Wijetunga I, Ingram N, Marston G, Prasad R, Markham AF, et al. Development of orthotopic tumour models using ultrasound-guided intrahepatic injection. *Sci Rep.* 2019; 9: 9904.
25. Bou About G, Thiebault E, Wattenhofer-Donze M, Jacobs H, Guimond A, Sorg T, et al. Ultrasound-Guided Approaches to Improve Orthotopic Mouse Xenograft Models for Hepatocellular Carcinoma. *Curr Protoc Mouse Biol.* 2019; 9: e62.
26. Dacek MM, Veach DR, Cheal SM, Carter LM, McDevitt MR, Punzalan B, et al. Engineered Cells as a Test Platform for Radiohaptens in Pretargeted Imaging and Radioimmunotherapy Applications. *Bioconjug Chem.* 2021; 32: 649-54.
27. Orcutt KD, Nasr KA, Whitehead DG, Frangioni JV, Wittrup KD. Biodistribution and clearance of small molecule hapten chelates for pretargeted radioimmunotherapy. *Mol Imaging Biol.* 2011; 13: 215-21.
28. Wahl RL, Sgouros G, Iravani A, Jacene H, Pryma D, Saboury B, et al. Normal-Tissue Tolerance to Radiopharmaceutical Therapies, the Knowns and the Unknowns. *J Nucl Med.* 2021; 62: 23S-35S.
29. Santich BH, Cheal SM, Ahmed M, McDevitt MR, Ouerfelli O, Yang G, et al. A Self-Assembling and Disassembling (SADA) Bispecific Antibody (BsAb) Platform for Curative Two-step Pretargeted Radioimmunotherapy. *Clin Cancer Res.* 2021; 27: 532-41.
30. Chandler CS, Bell MM, Chung SK, Veach DR, Fung EK, Punzalan B, et al. Intraperitoneal Pretargeted Radioimmunotherapy for Colorectal Peritoneal Carcinomatosis. *Mol Cancer Ther.* 2022; 21: 125-37.
31. McInnes EF, Mann P. Background lesions in laboratory animals : a color atlas. Edinburgh: Elsevier; 2012.
32. Orcutt KD, Rhoden JJ, Ruiz-Yi B, Frangioni JV, Wittrup KD. Effect of small-molecule-binding affinity on tumor uptake in vivo: a systematic study using a pretargeted bispecific antibody. *Mol Cancer Ther.* 2012; 11: 1365-72.
33. Le Roux A, Fung E, Xu H, Burnes Vargas D, Rinne SS, Guo H-f, et al. Anti-GPA33 Pretargeted Radioimmunotherapy (PRIT) of Colorectal Cancer (CRC) Using a Self-Assembling and Dis-Assembling (SADA) Bispecific Antibody to deliver ¹⁷⁷Lu-Bivalent Benzyl-DOTA. *J Nucl Med.* 2024; 65: 241233.
34. Han BS, Ji S, Woo S, Lee JH, Sin JI. Regulation of the translation activity of antigen-specific mRNA is responsible for antigen loss and tumor immune escape in a HER2-expressing tumor model. *Sci Rep.* 2019; 9: 2855.
35. Zhou T, Wang HW. Antigen Loss after Targeted Immunotherapy in Hematological Malignancies. *Clin Lab Med.* 2021; 41: 341-57.

36. Meirrow D, Nugent D. The effects of radiotherapy and chemotherapy on female reproduction. *Hum Reprod Update*. 2001; 7: 535-43.
37. Wallace WH, Shalet SM, Hendry JH, Morris-Jones PH, Gattamaneni HR. Ovarian failure following abdominal irradiation in childhood: the radiosensitivity of the human oocyte. *Br J Radiol*. 1989; 62: 995-8.
38. Lushbaugh CC, Casarett GW. The effects of gonadal irradiation in clinical radiation therapy: a review. *Cancer*. 1976; 37: 1111-25.
39. Clement SC, Kraal KC, van Eck-Smit BL, van den Bos C, Kremer LC, Tytgat GA, et al. Primary ovarian insufficiency in children after treatment with ¹³¹I-metaiodobenzylguanidine for neuroblastoma: report of the first two cases. *J Clin Endocrinol Metab*. 2014; 99: E112-6.
40. Teh WT, Stern C, Chander S, Hickey M. The impact of uterine radiation on subsequent fertility and pregnancy outcomes. *Biomed Res Int*. 2014; 2014: 482968.
41. Aguirre N, Veach D, Guo H-f, Espinosa-Cotton M, Fung E, Xu H, et al. Dose escalation and curative therapy of colorectal cancer with anti-GPA33 Self-Assembling and Disassembling (SADA) Actinium-225 Alpha Pretargeted Radioimmunotherapy. *J Nucl Med*. 2024; 65: 241791.

TABLES

Table 1. Three-step DOTA-PRIT estimated mean absorbed doses and therapeutic indices (tumor-to-normal tissue mean absorbed dose ratios) with monovalent [¹⁷⁷Lu]Lu-ABD and bivalent [¹⁷⁷Lu]Lu-Gemini radiohaptens in nude mice bearing orthotopic SW1222-luc CRC liver metastasis xenografts.

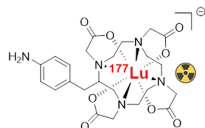
Pretargeting interval	¹⁷⁷ Lu]Lu-ABD (3.7 MBq , 0.4 nmol)				¹⁷⁷ Lu]Lu-Gemini (3.7 MBq , 0.2 nmol)			
	24h		48h		24h		48h	
	Estimated mean absorbed dose (cGy/MBq)	Therapeutic index	Estimated mean absorbed dose (cGy/MBq)	Therapeutic index	Estimated mean absorbed dose (cGy/MBq)	Therapeutic index	Estimated mean absorbed dose (cGy/MBq)	Therapeutic index
Tumor	32.88	/	11.82	/	125.43	/	119.88	/
Blood	2.14	15	1.54	8	3.50	36	2.40	50
Heart	1.39	24	0.65	18	3.76	33	3.58	34
Lungs	2.44	13	1.00	12	5.53	23	8.87	14
Normal liver	3.14	10	1.36	9	7.68	16	5.85	20
Spleen	2.28	14	1.04	11	6.24	20	5.31	23
Stomach	0.49	67	0.28	42	2.00	63	0.81	147
Small intestine	0.74	45	1.08	11	2.16	58	1.36	88
Large intestine	2.14	15	1.33	9	4.20	30	1.72	70
Kidneys	6.94	5	6.80	2	13.52	9	13.23	9
Muscle	0.49	68	0.19	62	1.00	125	0.70	171
Bone	2.42	14	0.22	53	1.61	78	0.84	143
Ovaries	2.38	14	1.03	11	6.83	18	3.66	33
Uterus	4.05	8	1.78	7	10.27	12	6.21	19

Table 2. GPA33 immunohistochemistry (IHC) signal positivity in recurrent hepatic tumors and extrahepatic metastases in nude mice (M1–M5) treated with three-step DOTA-PRIT with monovalent [¹⁷⁷Lu]Lu-ABD (Group 1 (G1), 3 therapy cycles, 1 week apart) and bivalent [¹⁷⁷Lu]Lu-Gemini (Group 2 (G2), single therapy cycle) (experimental protocol in Figure 5A).

Mouse #	Organs	IHC Signal Positivity	Survival (days)	Treatment
G1M1	Recurrent liver mass	>90%	64	[¹⁷⁷ Lu]Lu-ABD
	Small intestine	70%		
	Axillary lymph node	>90%		
	Diaphragm	>90%		
G1M2	Recurrent liver mass	5%		
G2M1	Recurrent liver mass	70%	81	
G2M2	Recurrent liver mass	>90%	113	[¹⁷⁷ Lu]Lu-Gemini
G2M3	Recurrent liver mass	>90%		
	Pancreas	20%		
G2M4	Liver tumor scar tissue	NA	81	
G2M5	Liver minimal residual viable tumor cells	>90%	68	[¹⁷⁷ Lu]Lu-Gemini
	Spinal cord	>90%		
	Mesometrium minimal viable tumor cells	>90%		
G3M3	Liver mass in control mouse	>90%	11	no BsAb/[¹⁷⁷ Lu]Lu-ABD

FIGURES

A

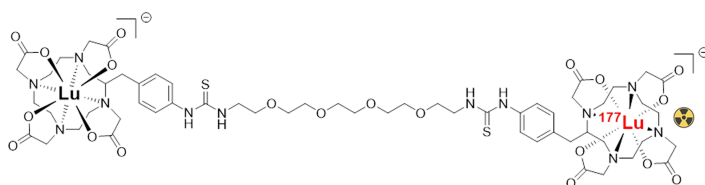
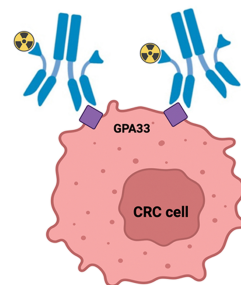


Monovalent [¹⁷⁷Lu]Lu-ABD hapten

Chemical Formula: C₂₃H₃₅N₅O₈

Molecular Weight: 509.56 (without radioisotope)

Molecular Charge = -1

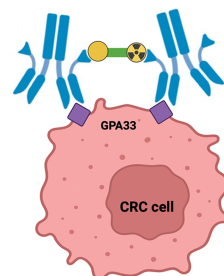


Bivalent "Gemini" [¹⁷⁷Lu]Lu-DOTA hapten

Chemical Formula: C₅₈H₉₀N₁₂O₂₀S₂

Molecular Weight: 1339.54 (without radioisotope)

Molecular Charge = -2



B

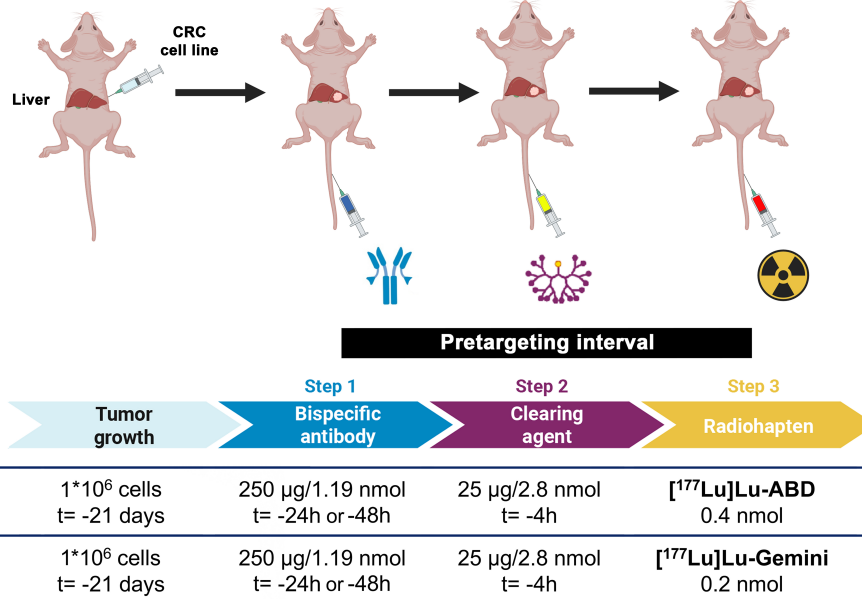


Figure 1. DOTA-based pretargeted radioimmunotherapy (DOTA PRIT) using monovalent and bivalent ¹⁷⁷Lu-labeled radiohaptens. A. Concept of avidity enhancement. [¹⁷⁷Lu]Lu-Gemini is a symmetrical dimer of ABD and forms highly stable complexes with a variety of radiometals (β and α-emitters). Gemini potentially allows cooperative binding, with both DOTA binding with the BsAb scFv C825 anti-(M) ABD site. The Gemini radiohapten precursor is initially radiometallated with ¹⁷⁷Lu, and the remaining empty DOTA chelators then filled with nonradioactive ¹⁷⁵Lu. Non-radioactive lutetium backfilling is necessary, as both DOTA must be metal bound (M-DOTA) to be recognized by the antibody on either side, allowing for cooperative binding and enhanced retention at the cell surface. **B.** Three-step DOTA PRIT protocol.

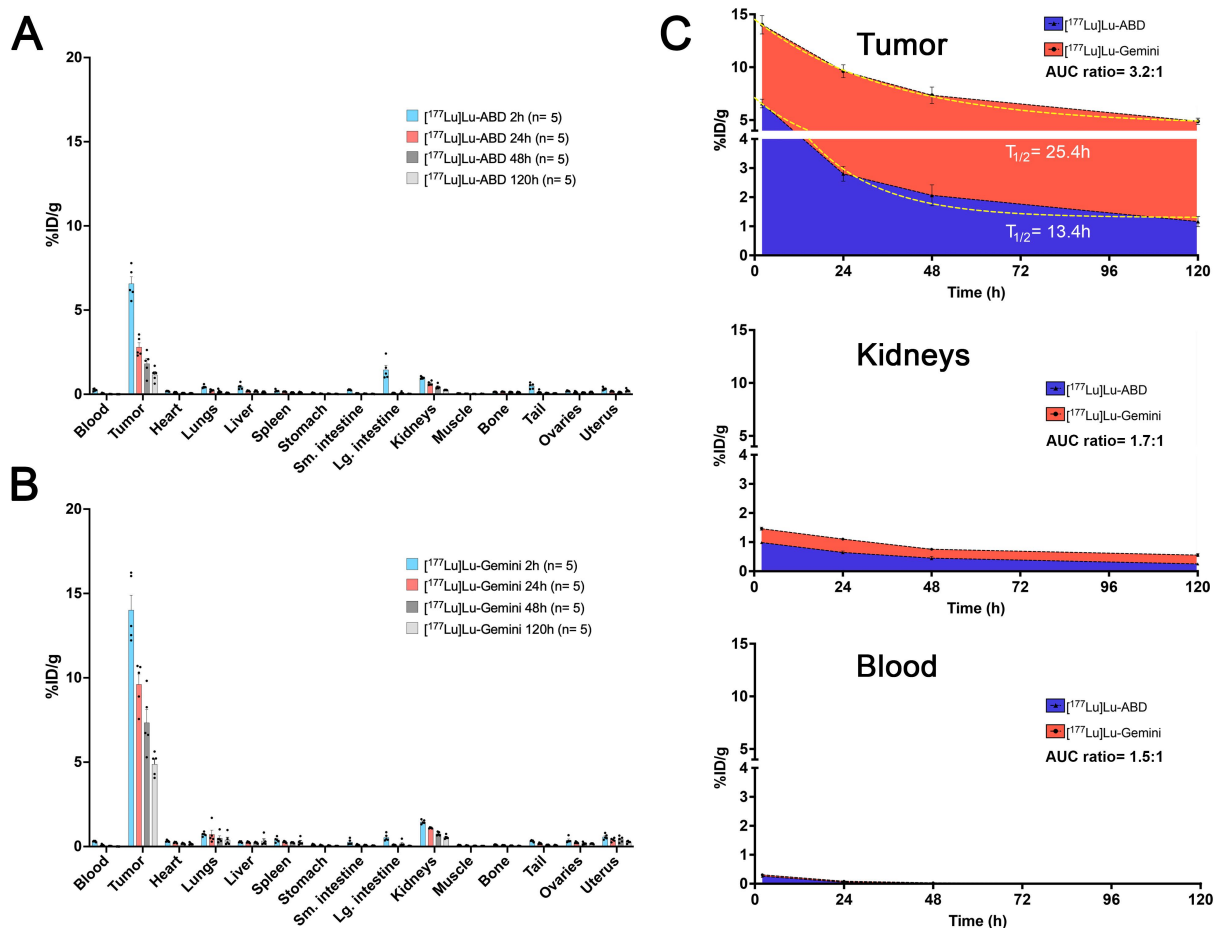


Figure 2. Monovalent $[^{177}\text{Lu}]\text{Lu-ABD}$ and bivalent $[^{177}\text{Lu}]\text{Lu-Gemini}$ three-step DOTA-PRIT ex vivo biodistribution comparison. A. $[^{177}\text{Lu}]\text{Lu-ABD}$ (3.7 MBq, 0.4 nmol) and **B.** $[^{177}\text{Lu}]\text{Lu-Gemini}$ (3.7 MBq, 0.2 nmol) three-step DOTA-PRIT ex vivo biodistribution. Values are represented as means, and error bars represent standard error of the mean (SEM). **C.** Area under the curve (AUC) analysis of ex vivo biodistribution for the tumor, kidneys, and blood. The longer biological half-life of $[^{177}\text{Lu}]\text{Lu-Gemini}$ on the tumor ($T_{1/2} = 25.4\text{ h}$) and higher plateau (4.5 %ID/g) compared with $[^{177}\text{Lu}]\text{Lu-ABD}$ ($T_{1/2} = 13.4\text{ h}$, plateau: 1.3 %ID/g) better aligns with the longer decay period of the therapeutic radioisotope (lutetium-177 half-life: 6.7 days), increasing tumor exposure time with a higher tumor activity retention (3.5-fold higher $[^{177}\text{Lu}]\text{Lu-Gemini}$ plateau value compared with $[^{177}\text{Lu}]\text{Lu-ABD}$). The dashed yellow lines on the tumor graph of subfigure C represent non-linear fit one-phase decay curves for $[^{177}\text{Lu}]\text{Lu-ABD}$ ($R^2 = 0.91$) and $[^{177}\text{Lu}]\text{Lu-Gemini}$ ($R^2 = 0.86$) tumor biodistribution data.

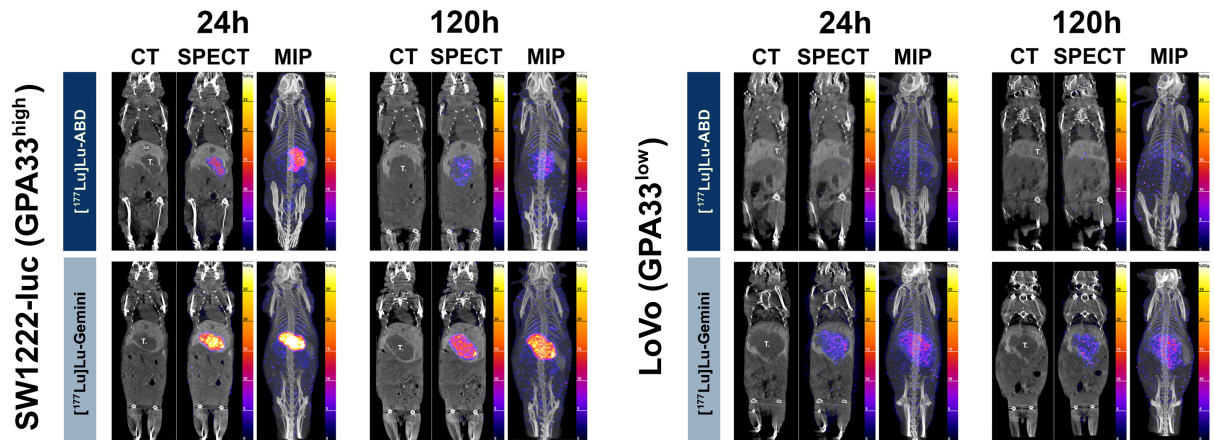


Figure 3. DOTA-PRIT SPECT/CT studies with high GPA33-positive (SW1222-luc) and low GPA33-positive (LoVo) CRC liver metastasis tumor-bearing mice. Coronal multiplanar reconstruction (MPR) and maximum intensity projection (MIP) SPECT images acquired 24 h and 120 h after 44.4 MBq injection of [¹⁷⁷Lu]Lu-ABD (0.4 nmol) and [¹⁷⁷Lu]Lu-Gemini (0.2 nmol). High SW1222-luc tumor uptake is noted on the 24 h SPECT images of both [¹⁷⁷Lu]Lu-ABD and [¹⁷⁷Lu]Lu-Gemini, with higher tumor retention of [¹⁷⁷Lu]Lu-Gemini at 120 h. In LoVo tumors, superior tumor targeting and retention are noted with [¹⁷⁷Lu]Lu-Gemini, compared with [¹⁷⁷Lu]Lu-ABD which shows negligible tumor uptake. T.: liver tumor; GB: gallbladder; Spl.: spleen.

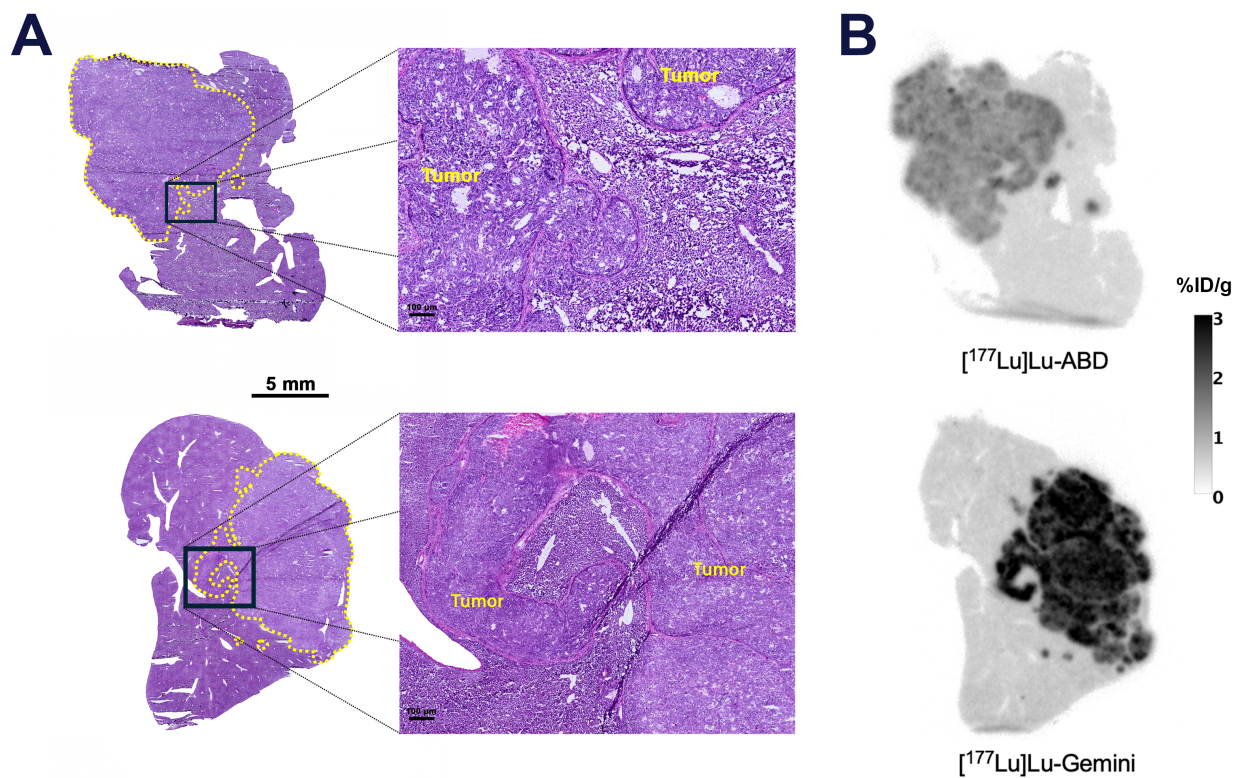


Figure 4. Quantitative autoradiography (QAR). **A.** Hematoxylin and eosin (H&E) micrograph of optimal cutting temperature (OCT)–frozen SW1222-luc hepatic tumors (circled in yellow), and **B.** concurrent QAR image 5 days after 44.4 MBq injection of [¹⁷⁷Lu]Lu-ABD (0.4 nmol) and [¹⁷⁷Lu]Lu-Gemini (0.2 nmol). Higher uptake is noted in the [¹⁷⁷Lu]Lu-Gemini tumor (mean %ID/g ± SD throughout the tumor: 2.1 ± 0.4 %ID/g) compared with [¹⁷⁷Lu]Lu-ABD (mean %ID/g ± SD throughout the tumor: 1.1 ± 0.2 %ID/g).

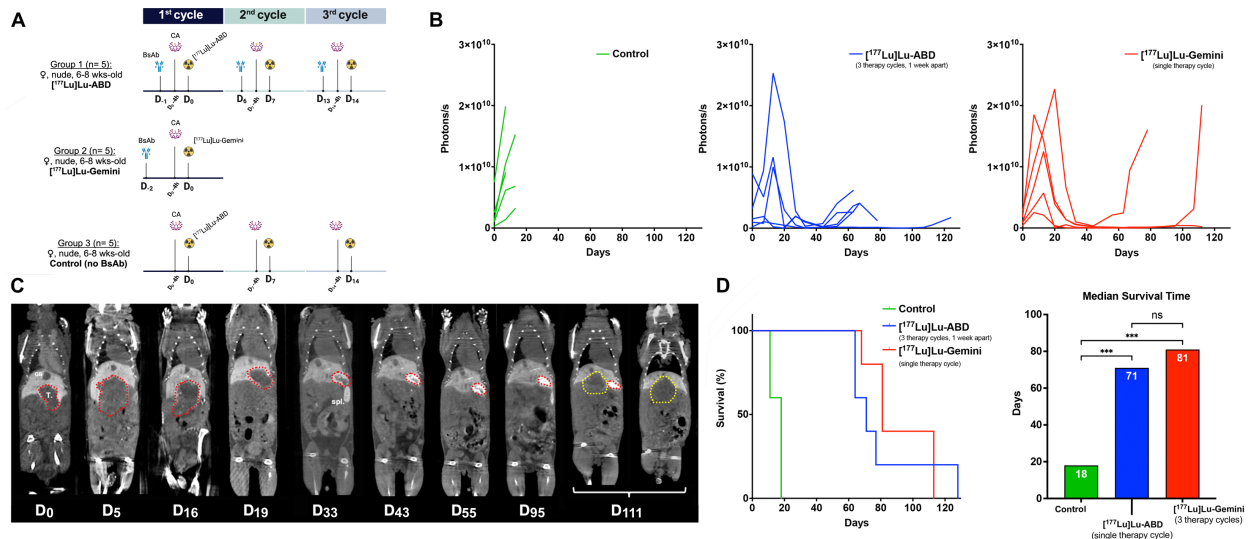


Figure 5. Three-step DOTA-PRIT experiment. **A.** Experimental three-step DOTA-PRIT protocol (with estimated tumor mean absorbed doses of 44 Gy and 53 Gy for 3 therapy cycles of [177Lu]Lu-ABD (group 1) and a single cycle of [177Lu]Lu-Gemini (group 2), respectively). **B.** Serial in vivo bioluminescence imaging (BLI). **C.** Serial coronal multiplanar reconstruction (MPR) CT images of a representative mouse treated with [177Lu]Lu-ABD DOTA-PRIT (same mouse as in Figure 3). The initial hepatic tumor is circled in red, and the recurrent tumor in yellow. The 2 coronal images at D₁₁₁ have been acquired at different coronal levels. T.: tumor; GB: gallbladder; spl.: spleen. **D.** Kaplan–Meier survival curves and median survival histograms. Median survival times were compared using the log-rank (Mantel-Cox) test. ns: not statistically significant; *** $p \leq 0.001$.

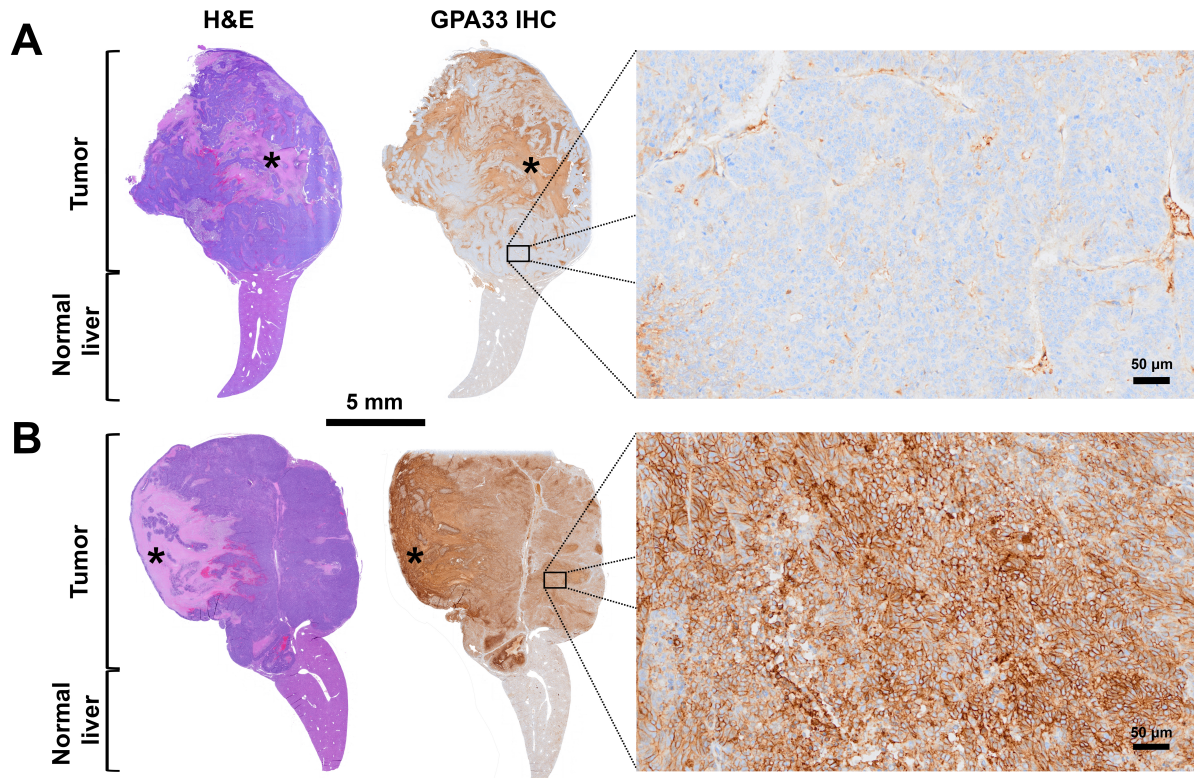


Figure 6. GPA33 differential expression in recurrent liver tumors post-three-step DOTA-PRIT (experimental three-step DOTA-PRIT protocol in Figure 5A). **A.** Representative hematoxylin and eosin (H&E) micrograph (left) and GPA33 immunostaining (right) of a recurrent GPA33(-) liver tumor 64 days post [¹⁷⁷Lu]Lu-ABD three-step DOTA-PRIT (G1M2 in Table 2). High magnification on viable cellular areas of the tumor shows negligible membranous GPA33 expression (5% immunohistochemistry (IHC) signal positivity). **B.** Representative H&E micrograph (left) and GPA33 immunostaining (right) of a recurrent GPA33(+) hepatic tumor 113 days post-[¹⁷⁷Lu]Lu-Gemini three-step DOTA-PRIT (G2M3 in Table 2). High magnification on viable cellular areas of the tumor shows diffuse and strong, membranous GPA33 expression (90% IHC signal positivity). Large necrotic areas, which show non-specific staining on IHC, are marked with an asterisk.